IOPscience iopscience.iop.org

Home Search Collections Journals About Contact us My IOPscience

Spontaneous and laser-enhanced halogen etching of GaAs(110)

This article has been downloaded from IOPscience. Please scroll down to see the full text article.

1998 J. Phys.: Condens. Matter 10 7723

(http://iopscience.iop.org/0953-8984/10/35/007)

View the table of contents for this issue, or go to the journal homepage for more

Download details:
IP Address: 171.66.16.209
The article was downloaded on 14/05/2010 at 16:42

Please note that terms and conditions apply.

J. Phys.: Condens. Matter **10** (1998) 7723–7742. Printed in the UK PII: S0953-8984(98)93179-4

Spontaneous and laser-enhanced halogen etching of GaAs(110)

B Y Han and J H Weaver

Department of Materials Science and Chemical Engineering, University of Minnesota, Minneapolis, MN 55455, USA

Received 9 November 1997

Abstract. We review studies of surface morphologies associated with Cl and Br etching of GaAs(110) via thermal and laser activation, with an emphasis on the former. Using atomic-resolution scanning tunnelling microscopy, we examine the chemisorption structures, etch pit development and growth on terraces, step etching, the concentration dependence of various etching pathways, and the etching yields in the temperature range of 300–800 K. Surface structural changes are correlated with the underlying reaction processes and the stabilities of steps. Etch pit morphologies achieved by nanosecond laser-pulse irradiation of Br-covered GaAs(110) are compared with those obtained in spontaneous etching. We discuss etching mechanisms in light of the observed differences in etching morphology.

1. Introduction

Dry etching using halogens plays an important role in microelectronic device fabrication [1]. In this context, it is important to understand how molecular halogens such as Cl_2 and Br_2 interact with semiconductor surfaces and how such reaction parameters as surface concentration, temperature and photon irradiation affect desorption products and surface morphology. Most investigations have emphasized gas-phase or surface reaction products [1–9]. While very important, they provide only indirect information about atomic-scale surface structures achieved during etching and how these structures influence reaction processes.

Here, we examine halogen etching of GaAs(110) with an emphasis on surface morphologies associated with thermal and laser activation [10–13]. Using atomic-resolution scanning tunnelling microscopy (STM), we first consider the equilibrium halogen chemisorption structures at room temperature. We then discuss etching at steps and the development of etch pits and their growth on terraces. Results obtained by controlled heating of partially halogenated surfaces reveal competition between various etching pathways. Analysis of these results gives the etching yields in the temperature range of 300–800 K. Finally, we consider laser-enhanced etching and discuss reaction mechanisms by comparing etch pit morphologies to those obtained in thermal etching.

2. Experimental considerations

The experiments reviewed here were conducted in an ultrahigh vacuum chamber (base pressure of $\sim 6 \times 10^{-11}$ Torr) equipped with a Park Scientific Instruments scanning tunnelling

0953-8984/98/357723+20$19.50 © 1998 IOP Publishing Ltd

microscope. Mirror-like GaAs(110) surfaces were prepared by cleaving posts that were Zn doped at 1×10^{18} cm^{-3}. Halogen molecules were produced by electrochemical cells formed by fusing mixtures of Ag and Cd halides [14]. During exposure, the source was ~2 cm from the GaAs(110) surface. Embedded silver and platinum leads provided electrical contact. When a voltage was applied, the halogen ions diffused to the positively biased Pt mesh where they combined and desorbed as neutral molecules. Exposures were calibrated by Faraday's first law. The currents used here were 6 μA or 60 μA, corresponding to a release rate of 1.8×10^{13} or 1.8×10^{14} molecules per second. Exposures are quoted as the product of the current and time, mA s. The flux incident upon the sample is specific to our geometry and sticking coefficients depend on the conditions and temperature of the surface [15]. In our experimental configuration, a halogen exposure of ~1.8 mA s saturated a GaAs(110) surface at 300 K. Heating was provided by a tungsten filament mounted on the back of the sample holder. Temperatures were monitored with a chromel–alumel thermocouple and an optical pyrometer.

In laser-enhanced etching, a frequency-doubled Nd-YAG laser emitting 2.3 eV (532 nm) photons with a pulse duration of ~6 ns and pulse intensities between 1 and 50 mJ cm^{-2} was used to irradiate a Br-covered GaAs(110). The pulse energy was measured with a pyrolytic power meter (Scientech 010), and the spatial profile was determined with a photodiode. Precautions were taken to ensure uniformity of irradiation over the surface (1 mm aperture in the laser cavity to transmit only the Gaussian TEM_{00} mode and a dispersive lens to spread the beam). The laser light was coupled into the chamber through a Pyrex window.

The STM images were acquired at room temperature in the constant current mode with tunnelling currents of 100–200 pA and bias voltages of $\pm$(1.5–3.5) V. The images presented here have $[1\bar{1}0]$ running from lower right to upper left unless otherwise specified. They are not corrected for drift, and this accounts for some skewing.

3. Spontaneous halogen etching

We have explored two ways to achieve thermal etching. In one, the sample was exposed to obtain an initial halogen coverage prior to a heating cycle. Under the expose/heat cycles, etching was done in the range 500–775 K [11, 12]. The typical temperature ramp-up time was ~7 min, and the sample was kept at the maximum temperature for 20 min before cooling. An expose/heat cycle achieves conditions representative of temperature programmed desorption (TPD) [2, 3]. The stepwise increase of the end-point temperature yields information about the activation of different processes. By varying the initial halogen coverage, we have been able to study coverage-dependent etch morphologies and related etching pathways.

In the second process, the sample was held at a fixed temperature (550–775 K) during halogen exposure [10]. In this continuous etching case, the surface morphology reflects the balance between halogen uptake and etching. It has been used to study etching at a particular temperature and, to some extent, it complements molecular beam scattering experiments [1, 4, 5] that emphasize gas-phase products.

3.1. Br and Cl adsorption on GaAs(110), 300–450 K

Molecular adsorption of bromine and chlorine is dissociative on GaAs(110). For Br–GaAs(110), photoemission studies [7] have revealed two components in the Br 3d core level emission after adsorption at 300 K. These results were interpreted in terms of Br bonding to Ga and As surface atoms. For Cl–GaAs(110), early studies suggested bonding

only to As [16], but recent studies of desorption products [17] and surface reaction species [8, 9] have concluded that Cl bonds to both As and Ga. Real space imaging using high-resolution scanning tunnelling microscopy has provided definitive support for the latter [10].

Figures 1(a)–(d) show chemisorption structures representative of exposure to Br or Cl. Figure 1(a) was obtained after exposure to 0.2 mA s of Br_2 at 300 K. Two distinct Br-induced features are clearly evident, labelled A and B and depicted in figure 2. The A features form 1–1.2 Å high islands where the spacing between features is 5.6 Å along [001] and 4 Å along $[1\bar{1}0]$. They appear within a rectangle defined by four As atoms, reflecting adatoms bonded to Ga sites, denoted Br–Ga. Their exact position within the rectangle is not known since STM images reflect charge distributions rather than nuclear positions. Theoretical calculations suggest that halogens tie up the surface Ga dangling bonds [18, 19]. The B features are 2.1–2.3 Å high when measured with negative sample bias and ~2.6 Å when measured with positive sample bias. They reflect Br adatoms bonded to As sites, denoted Br–As. Two such defects are sketched in the island on the left of figure 2. At low exposure at 300 K, they appear as defects within A-type islands, centred above surface As atoms.

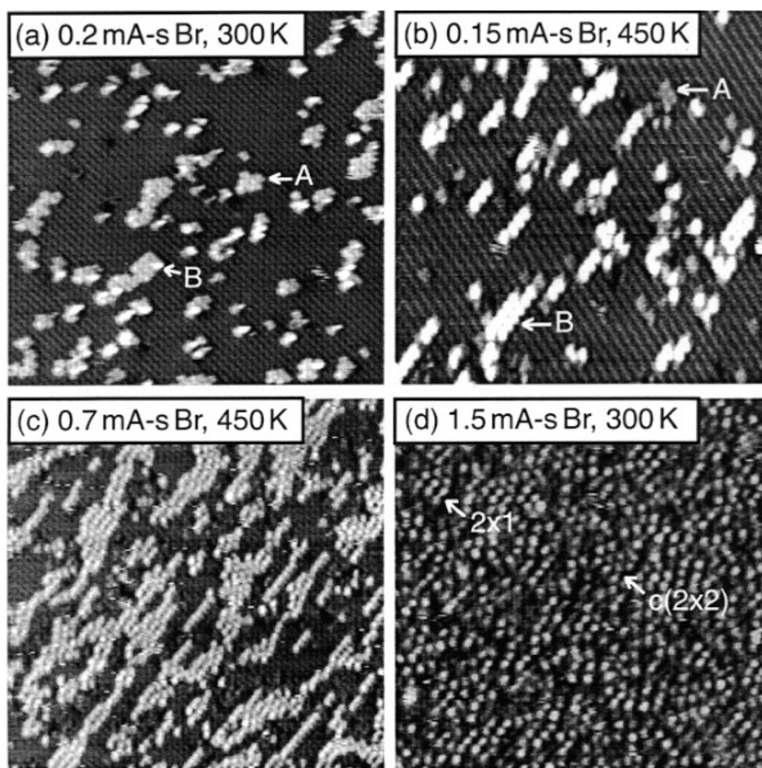

Figure 1. (a) Adsorption structures for Br on GaAs(110) showing A-type islands and B-type defects within the islands. A-type features have local 1×1 symmetry. (b) Image obtained after exposure at 450 K showing linear chains elongated along [001]. (c) Image demonstrating coalescence of chains into islands. The bright features represent Br bonded to As sites, forming $2 \times 1/c(2 \times 2)$ islands. The 1×1 Br–Ga structures are obscured by higher Br–As features. (d) GaAs(110) after near-saturation exposure at room temperature. The overlayer consists of Br features with short-range 2×1 and $c(2 \times 2)$ structure, as marked by arrows. ((a) 300×300 Å^2; (b) 180×180 Å^2, (c) and (d) 250×250 Å^2.) (Adapted from [10] and [11].)

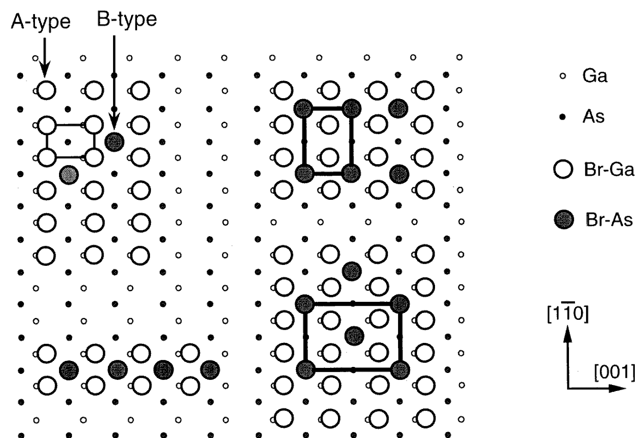

Figure 2. Model depicting the adsorption sites for Br and Cl on GaAs(110). The A-type islands have halogen-induced features within the rectangle formed by four As atoms. They reflect Br (Cl) bonded to Ga. The B-type features are located above the As atoms. Heating produces chains derived from A and B features elongated along [001], as shown at lower left. Extended exposures produce islands, as depicted on the right for the (2 × 1) and c(2 × 2) structures.

Figure 1(b) shows that exposure at 450 K enhances the formation of chains elongated along [001], as depicted at the lower left of figure 2. These linear chains, one or two rows wide, are composed of B-type features flanked on either side with one row of A-type features at lower height. Only the brighter B-type features are clearly visible in STM images of these structures. Dual bias images demonstrate that they are located over As rows for both biases, as when such features appear as minority species in A islands. In figure 1(b), some A-only features are also present.

Figure 1(c) shows that chains coalesce into islands with local (2 × 1) and c(2 × 2) symmetry composed of B features. The Br coverage is ∼0.3 ML in figure 1(c). We have not found B-type features that occupy two adjacent As sites along a zig-zag row for any coverage studied, in contrast to (1 × 1) A features that form after exposure at room temperature.

Structures similar to those in figures 1(b) and 1(c) have been obtained by room temperature exposure with subsequent annealing to 400–450 K. This indicates that enhanced diffusion allows them to sample optimal thermodynamic structures. Theoretical calculations have suggested that the energy per unit cell for chain structures is probably lower than for A-type islands [18]. This, together with a relatively low diffusion barrier (∼0.5 eV) for halogen adatoms along [1$\bar{1}$0] on GaAs(110) [20], accounts for the evolution of adsorption structures with temperatures.

A few dark spots are also visible in images taken after halogen exposure (figure 1). Some of them probably result from adsorption-induced etching. Their areal density showed little change when Br-covered surfaces were heated to 450 K for 10 min. This temperature is below the threshold for Ga–Br desorption. Heating to 500 or 600 K increased their density.

Figure 1(d) reproduces an image for a surface that is almost saturated, with a coverage of ∼0.6 ML. Note that the maximum coverage is 0.75 ML since adjacent As sites on a zig-zag row cannot be simultaneously occupied. In figure 1(d), small domains of (2 × 1) and c(2 × 2) character are visible. Ordering of the adsorption structure can be enhanced by annealing to 400–450 K.

Theoretical treatments of surface bonding using a linear combination of atomic orbitals approach [17] focused on the bonding, nonbonding, and antibonding levels for Ga–Cl and As–Cl 'surface molecules'. These authors concluded that Cl bonded to both Ga and As. Khoo and Ong [19] used a semi-empirical molecular-orbital method to determine the equilibrium bonding structure for dilute Cl coverages. They found coexistence of Cl–Ga and Cl–As bonding configurations where the latter appeared in the midst of Cl–Ga. For Cl–Ga bonding, the adatom would attach to the surface Ga dangling bond. For Cl–As bonding, the Cl atom would be nearly atop the surface As atom. Corkill and Chelikowsky [18] used *ab initio* pseudopotential methods within the local density approximation to calculate total energies for different adsorption configurations. For a homogeneous overlayer, their results showed that A islands (consisting of Cl–Ga) are lower in energy by $\sim$1.2 eV/Cl atom compared to B islands (consisting of Cl–As). Their results also suggested that the chain structures reflect an attractive Cl–Cl pair interaction between adjacent A- and B-type Cl in the linear chain geometry. We conclude that theory and experiment are in good accord regarding Cl and Br adsorption on GaAs(110).

3.2. Etch pit development: pairwise removal of Ga–As

Investigations of the development and growth of terrace etch pits provide insights into the underlying reaction processes. Figure 3(a) shows the morphology obtained after heating to 650 K for a surface that had an initial Br coverage of 0.005 ML. The surface is decorated with small pits that appear as dark depressions in the zig-zag rows. They are one layer deep. Most of them represent removal of one to three Ga–As pairs. Those that are one row wide do not exceed three unit cells in length along $[1\bar{1}0]$. Bright spots at pit edges reflect residual Br adatoms that are mobile at 650 K but are frozen in pit boundary sites as the sample cools. For most of the pits in figure 3(a), the ends show different, but nonetheless well defined, appearances when viewed with higher resolution. This is to be expected if Ga–As pairs are removed along $[1\bar{1}0]$ since one end would be Ga terminated and the other would be As terminated. Note that heating to 650 K of GaAs(110) that was free of Br did not introduce defects of the sort identified in figure 3(a).

Dual-bias imaging can help identity which type of atom bounds a line vacancy since occupied-state images reveal the As sublattice while unoccupied-state images reveal the Ga sublattice [21]. Figure 3(b) shows high-resolution, dual-bias images for a small pit. The images were acquired simultaneously using alternating line-scans in either bias so that drift would not affect the atomic registry. Inspection reveals that the main vacancy row of figure 3(b) is bounded by an As atom at the upper end and a Ga atom at the lower end. This corresponds to the removal of two Ga–As pairs, as described the model below the images. Inspection also shows that one Ga–As pair is missing on the row to the left of the main vacancy. This pair vacancy is bounded by an As atom at the upper end and a Ga atom at the lower end. It could have been formed independently on the terrace or through a branching event at the main row, with subsequent diffusion away from the parent unit.

Analysis of a large number of pits localized to one or two zig-zag rows shows that approximately 80% were composed of pair vacancies. Hence, the main growth channel involves pairwise removal from surface lattice sites. The desorption of Ga bromide is accompanied by the release of an As atom that can diffuse until it encounters another As atom where it forms volatile As_2 (or As_4) and desorbs. The absence of preferred even- or odd-numbered pairs suggests that the pit growth increment is a single pair.

While most small pits consist of pair vacancies, there are some that reflect an odd number. The arrow in figure 3(a) points to an odd-length vacancy, corresponding to a pit

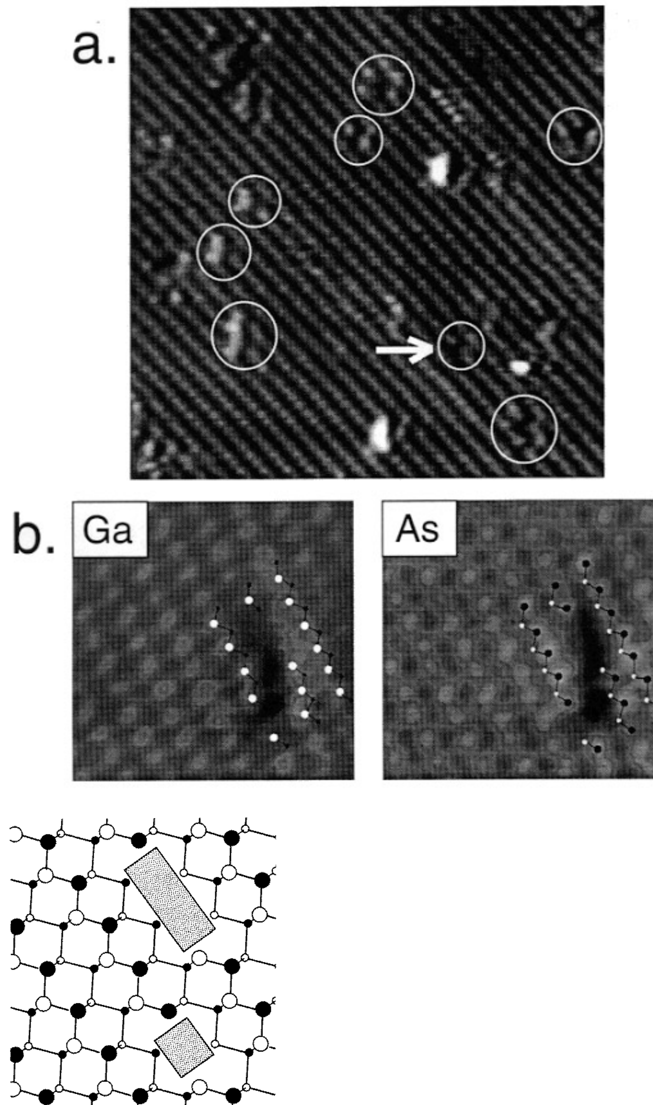

Figure 3. The initial stages of etching corresponds to terrace pit creation. Small single-layer deep etch pits are clearly visible in (a), some of which are circled. They appear as dark features that disrupt [1$\bar{1}$0] atomic rows. The etch pit marked by an arrow probably reflects a Ga–As–Ga tri-vacancy. (b) Dual-bias atomic-scale images of a small etch pit. The main vacancy row corresponds to the removal of two Ga–As pairs with an As atom at the upper end and a Ga atom at the lower end. The apparent positions of some As and Ga atoms are marked by black and white dots in their respective sublattice. A single Ga–As pair vacancy appears to the left of the pit. (c) Ball and stick model of the etch pit in (b). ((a) 150×150 Å^2, (b) 50×50 Å^2.) (Adapted from [12].)

that is 8 Å long and one row wide. The bright and symmetric appearance of its ends in the As-sublattice image suggests that it is a Ga–As–Ga trivacancy [12]. One way that an odd-number vacancy could be produced would involve capture of a mobile As adatom by an even-numbered vacancy.

3.3. Onset of thermal etching

Insights into the activation of desorption processes can be gained by heating halogen-covered GaAs(110) to incrementally higher temperatures [11]. Figures 4(a) and 4(b) are images of the surface in figure 1(d) after heating to 500 and 600 K. Heating to 500 K significantly reduced the density of bright features attributed to Br–As sites. The dark patches reflect single-layer etch pits (marked II); their emergence represents the onset of thermally activated etching. These pits expand in size upon heating to 600 K. In figure 4(b), the Br–As features have nearly vanished, except at pit boundaries, and clean surface zig-zag rows have reappeared as the Br concentration has decreased. Lighter areas represent the original surface (marked I) and darker areas reveal the second layer (marked II). The top layer is decorated with irregular structures due to Br–Ga and undesorbed As released during etching.

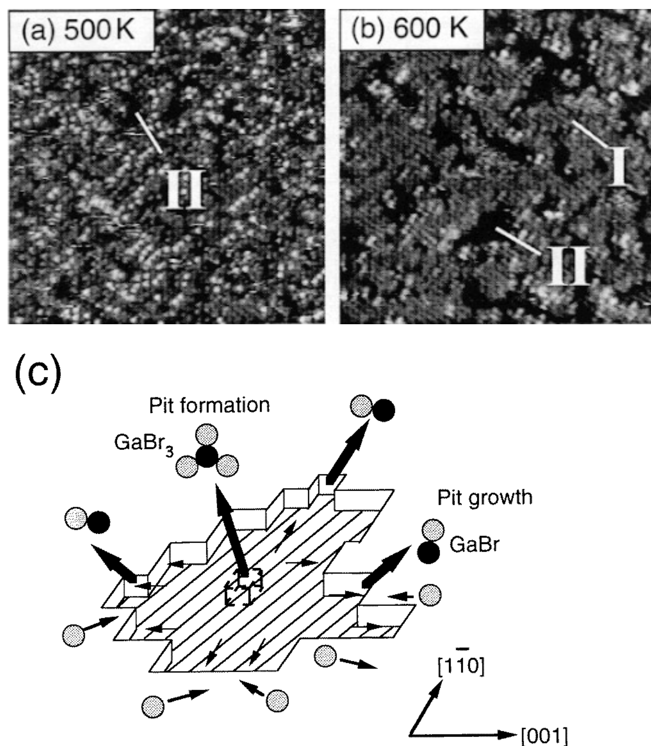

Figure 4. Images obtained after heating the saturated surface represented by figure 1(d) to 500 K and 600 K. Areas marked I and II are portions of the top and etched layer, respectively. Pitting in (a) reflects the onset of thermally activated etching at ∼500 K. Significant pit growth occurs at ∼600 K. (c) A schematic of the surface processes. Terrace pitting is caused by $GaBr_3$ desorption while steps retreat primarily by GaBr desorption. The concentration of Br is almost zero on the exposed second layer. (280×280 Å^2 for both.) (Adapted from [11].)

The STM results show morphologies that represent two distinct etching stages, in agreement with TPD studies [2–4]. The first is characterized by development of single-layer terrace pits (∼500 K for Br) that are associated with the desorption of GaX_3 (X = Br, Cl) from terraces. Once created, a pit can elongate along $[1\bar{1}0]$ and can expand into adjacent rows, as depicted schematically in figure 4(c). Desorption of GaX (X = Br, Cl) from pit

edges, where substrate atoms are weakly bonded, sets in at ∼600 K. This process contributes to pit enlargement and accounts for most of the substrate material removal. Both processes release As from the surface lattice.

The evolving surface reveals the details of bonding, with terrace atoms being more tightly bound than those at steps or kinks. From TPD experiments with Cl–GaAs(001), French *et al* [2] derived desorption energies of ∼75 and ∼155 kJ mol^{-1} for $GaCl_3$ and GaCl. The trihalide channel has a lower reaction barrier but it is only accessible when there is a sufficient halogen concentration. The monohalide channel has less stringent requirements on concentration but it has a significantly higher desorption barrier.

The effective contributions of the GaX_3 and GaX desorption pathways depend on the instantaneous coverage. We have determined the ratio of these pathways for surfaces that had initial concentrations of 0.08 to 0.5 ML. The importance of the two pathways is manifested in the etch yield, i.e. the number of atoms removed per halogen atom. With GaX_3 etching, three halogen atoms participate in removal of one Ga atom, whereas GaX etching requires only one. An increased contribution of GaX_3 reduces the yield. Competition between the two can be described by a kinetic model where desorption of GaX and GaX_3 are independent processes; release of As from the surface lattice is treated as a spontaneous follow-up step that does not explicitly enter the rate equations [11]. Fitting to experiment for a range of initial Br coverages produces a branching ratio for the two channels. The results are shown in figure 5. The $GaBr_3$ contribution was lower than 1% for initial coverages below ∼0.1 ML, with an etch yield close to 2. The $GaBr_3$ contribution rose to 12% for an initial coverage of 0.5 ML and the etch yield decreased to ∼1.6.

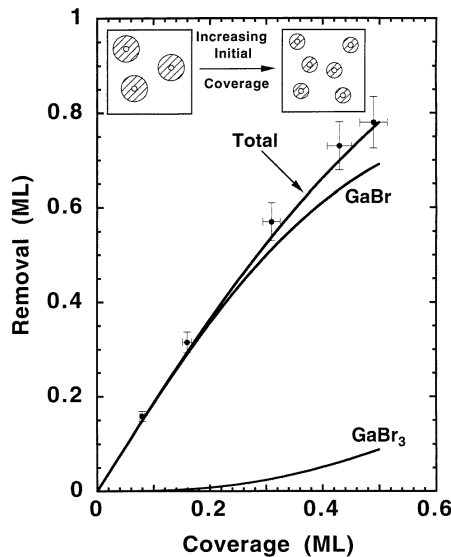

Figure 5. Plot of the total amount of material removed as a function of initial Br coverage, showing data points and the fit. Also shown are the amounts of removal for the GaBr and $GaBr_3$ channels, deduced from the kinetic model [11]. The proportion of removal via $GaBr_3$ increases with initial coverage. The inset depicts formation of more pits at higher initial coverage. At lower initial coverage, the vacancy islands are fewer but they are larger because step retreat dominates. Saturation coverage corresponds to 0.75 ML. (Adapted from [11].)

3.4. Etch pit growth and atom rebonding at pit boundaries

Steps constitute the boundaries of etch pits on terraces, and their atomic structures reflect the energies of removing atoms from their various bonding configurations. Figure 6 shows two typical images obtained after heating samples to 650 K that had initial Br coverages of 0.015 and 0.2 ML. Comparison to figure 3 reveals growth along the zig-zag rows and across them. Most pits of figure 6(a) extend over one to three rows and they are two to eight unit cells long, corresponding to the removal of 2–20 Ga–As pairs. All pits longer than three unit cells along [1$\bar{1}$0] cross at least two rows. Kinks are apparent on Ga- and As-edged [1$\bar{1}$0] steps. For example, the arrow labelled I identifies a kink in the Ga[1$\bar{1}$0] row. It reflects two missing Ga–As units. The arrow labelled II points to a kink in an As[1$\bar{1}$0] row that is three units in length, adjacent to a parent that is two rows wide. Analysis of hundreds of pits revealed that 60% have kinks on both sides. Of the remaining 40%, kink creation is favoured on the Ga[1$\bar{1}$0] side by a factor of about two, giving a bias in favour of Ga[1$\bar{1}$0] kinks of 54:46. The lack of preferred kinking on one side or the other is consistent with results by Patrin and Weaver [10] for continuous thermal etching in this temperature range, although they focused on pits that extended over six or more rows.

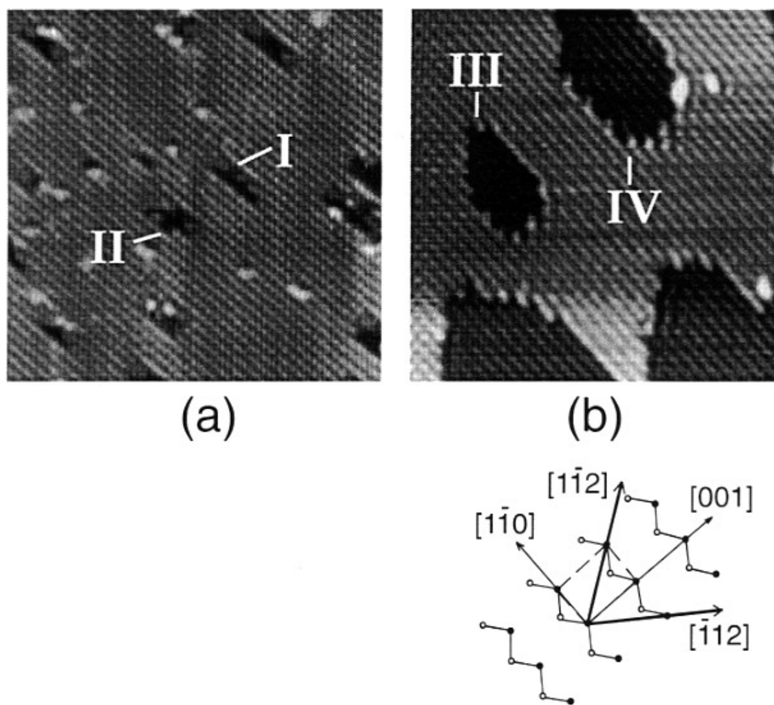

Figure 6. STM images of GaAs(110) etched at 650 K when the initial Br coverages are 0.015 ML (a) and 0.2 ML (b). Kinks on Ga and As[1$\bar{1}$0] steps in (a) are marked I and II. As the pits grow, they tend to exhibit hexagonal shapes established by segments of [1$\bar{1}$0] and $\langle 1\bar{1}2 \rangle$ steps, such as pits III and IV in (b). The principal directions are defined below the images. Misalignment reflects drift. ((a) 250×250 Å^2, and (b) 300×300 Å^2.) (Adapted from [12].)

Kink creation can occur at either end or the midpoints of a pit. Once formed, kinks such as I and II of figure 6(a) can grow along [1$\bar{1}$0]. Extended growth after creation tends

to align the ends of parent and daughter rows, and this makes it impossible to determine where the kink was formed. The kinks that are only a few units in length tended to appear at midpoints by roughly a factor of three compared to end points. Dual-bias imaging reveals that about 80% of the kinks correspond to removal of Ga–As pairs [12].

Heating a surface with an initial Br coverage of 0.2 ML to 650 K produces large, single-layer pits (figure 6(b)). These pits exhibit hexagonal shapes established by kinked segments of $[1\bar{1}0]$ and $\langle 1\bar{1}2\rangle$ steps. Two such pits are marked by III and IV in figure 6(b). The shape evolution is analogous to that observed in growth where an island composed of a few atoms is often ill defined but low energy facets are developed as it grows. (See schematic diagram for some principal surface directions. Misalignment is caused by thermal drift.) A few residual Br atoms decorate the pit edges. The $\langle 1\bar{1}2\rangle$ steps are terminated by both As and Ga atoms, as confirmed by dual-bias imaging [12]. The step lengths along $\langle 1\bar{1}2\rangle$ are appreciable. Such $\langle 1\bar{1}2\rangle$ steps represent a lower energy pit boundary than other steps such as [001], as confirmed by considerations based on local charge balance requirements (electron counting model) [22]. Some As$[1\bar{1}0]$ steps created by etching show bright spots that exhibit 4× periodicity (or, less frequently, 3× periodicity), as in pit IV. They might reflect local surface reconstructions similar to those found on GaAs(111) surfaces [23, 24], but their exact origin is not known.

The structure of extended pits can be deduced from dual-bias images such as those in figure 7. For this pit, the three rows to the right of the bright spot at upper left in the image are, respectively, As, As and Ga terminated. The registries of the two As atoms appear inclined to the left relative to the neighbouring zig-zag rows. We associate this distortion with As rebonding to second layer As at this $[1\bar{1}2]$ step, as depicted in the model. The two rows to the left of the Br feature are Ga and As terminated, respectively. While there is evidence for As rebonding, the experimental results are inconclusive regarding Ga rebonding, though such a process at a step is possible. Gallium dimerization has been reported at Ga-terminated GaAs(100) [25, 26], and Ga–Ga bonding has been deduced at single As vacancies on GaAs(110) [27, 28].

In the schematic diagram of figure 7, Ga-1 is adjacent to an As atom at the end of a pit whereas Ga-2 is part of the step. Analysis of a large number of etch pits showed that such alternation is typical [12]. This strongly suggests that etching is equally likely at Ga- and As-terminated vacancy rows. This is intriguing as one might expect from bond counting that a Ga atom adjacent to an As termination might be more strongly bound than a Ga atom that is itself the termination (the former has three backbonds and the latter has two). However, As atoms can rebond with their second-layer neighbours. This probably weakens the bond between the rebonded As atom and its Ga neighbour and facilitates the removal of the latter as GaBr. The validity of this intuitive picture remains to be verified. Model calculations would need to consider the transition states associated with Br atom(s) at relevant positions around the pit and the barriers for GaBr desorption.

The bright spot on the upper left edge of the pit of figure 7 is evident in both biases. It is due to a residual Br adatom that can be imaged because there are bonding and antibonding states of Br–Ga or Br–As that are accessible under our tunnelling conditions ($V_s = 1.9$–3.2 V) [10]. This Br adatom is atop an As atom and its location is labelled Br–As in the model beneath the image.

Pit growth is determined by desorption barriers for volatile species at the different step positions, subject to local Br concentrations. Simple considerations suggest that etching should be favoured along $[1\bar{1}0]$ where atoms are nominally twofold coordinated. Atoms at $[1\bar{1}0]$ steps are threefold coordinated. Even so, they are less well bound than atoms

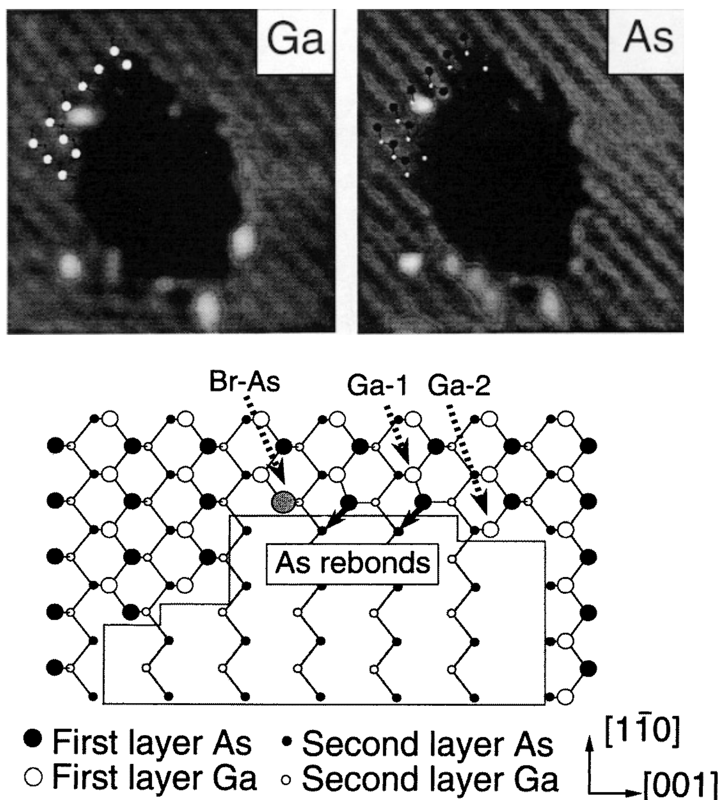

Figure 7. Dual-bias STM images of a large pit created when a surface having an initial Br coverage of ∼0.05 ML was heated to 650 K. The apparent positions of some As and Ga atoms are marked by black and white dots in their respective sublattices. The schematic represents the structure of the upper left edge of the pit. Arsenic atoms are depicted as rebonded with second-layer As atoms. The text discusses etching of Ga atoms from sites such as those labelled Ga-1 and Ga-2. (75 × 75 Å^2.) (Adapted from [12].)

on defect-free terraces. The statistics for kink creation on Ga[1$\bar{1}$0] and As[1$\bar{1}$0] suggest nearly equal overall energy barriers for desorption from the two steps. For a medium sized pit such as III in figure 6(b), at least five high-activation-energy kink events must have occurred after pit initiation because it extends over six rows. Elongation along [1$\bar{1}$0] would have been the dominant material removal channel, accounting for roughly 70 pairwise events. Unfortunately, it is not possible to deduce the energy difference between kinking and elongation since $GaBr_3$ desorption prevails in the former and GaBr desorption in the latter.

3.5. Expose/heat against continuous etching

When considering the details of pit formation, it is important to consider the concentration etchant on the surface. As noted above, the two competing channels for Ga removal have quite different requirements for Br (GaBr versus $GaBr_3$). In an experiment based on heating a pre-exposed surface, it must be remembered that Br tends to form islands (see figure 1).

Once formed, Br diffusion from centrally located sites is impeded by neighbouring Br atoms by site blocking. Accordingly, the concentration of Br remains high and such areas are favoured for pit formation and expansion across the rows.

Continuous etching at 500–650 K leads to simultaneous multilayer erosion [10] because the surface concentration is high and this high-concentration, low-barrier $GaBr_3$ channel is favoured. Such $GaAs_3$ desorption processes are less favoured in continuous etching at higher temperature with fixed (low) halogen fluxes because the surface concentration is lower. The balance between GaBr and $GaBr_3$ etching, and therefore the surface morphology, can be altered by varying the flux or temperature. The former changes the surface concentration at a given temperature and changes the balance of competing reaction channels. The effect of temperature is to alter not only the reaction rate of each channel, through the exponential, but also their relative importance through the concentration prefactor. Higher temperature corresponds to a lower surface concentration. Moreover, the temperature affects the surface structure as atoms attach and detach from steps and vacancies diffuse. In general, a low halogen flux and a high temperature favours 2D etching and a smoother surface.

3.6. GaAs(110) step etching

Cleaved GaAs(110) surfaces are characterized by large terraces with steps that tend to be aligned along $\langle 110\rangle$, $\langle 001\rangle$, and $\langle 112\rangle$. Step etching produces characteristic structures [10]. Figure 8(a) was obtained after continuous etching at 675 K. It shows a single height (SH) $[1\bar{1}0]$ step that crosses the image at the upper right and another that intersects a SH $[1\bar{1}2]$ step in the centre. The SH $[1\bar{1}0]$ steps are reasonably straight but there are kinks and regions that indicate etching into the upper or lower terrace. Near these steps, the etch pit density is approximately the same as on extended terraces. In contrast, $[1\bar{1}2]$ steps show significant etching. In figure 8(a), the original step location is still apparent but the terraces on both sides have been eroded.

The difference in SH $\langle 1\bar{1}2\rangle$ and $\langle 1\bar{1}0\rangle$ step reactivities reflects a combination of factors. First, atoms at $\langle 1\bar{1}0\rangle$ steps are threefold coordinated while those across $\langle 1\bar{1}0\rangle$ steps are nominally twofold coordinated. (Rebonding of atoms on $\langle 1\bar{1}2\rangle$ steps is possible, as discussed above.) Second, the diffusion of Br is anisotropic [20, 29], resulting in preferential transport along $\langle 1\bar{1}0\rangle$ relative to $\langle 001\rangle$. The higher Br delivery rate to the more reactive $\langle 1\bar{1}2\rangle$ steps contributes to the observed contrast.

Single height and double height (DH) steps etch differently. Figure 8(b) shows a SH $[1\bar{1}0]$ step at the left and a DH $[1\bar{1}2]$ step at the right after exposure to Br_2 at 725 K. The white line approximates the position of the original SH step. Note that this image is rotated relative to the others and $[1\bar{1}0]$ is along the x-axis, as indicated. Etching resulted in the retreat of the SH $[1\bar{1}2]$ step by approximately 500 Å. However, the step is not straight and large-scale deviations from linearity are evident. Figure 8(b) shows five fingers or peninsulas that extend to the right from the retreating SH $[1\bar{1}2]$ step. Each is terminated by a DH step since the DH step acts like a pinning fault. They are created at the retreating step edge when etching occurs into the lower terrace. These peninsulas have long sides that represent SH $[1\bar{1}0]$ steps. While etching into the peninsulas is slower than along $[1\bar{1}0]$, it accounts for the isolation of the SH etch regions near the position of the original step (one is located at lower left on the dashed line). The formation of rectangular etch pits in the lower terrace can be understood by noting that DH faults create steps that can flow along $[1\bar{1}0]$ into the lower terrace.

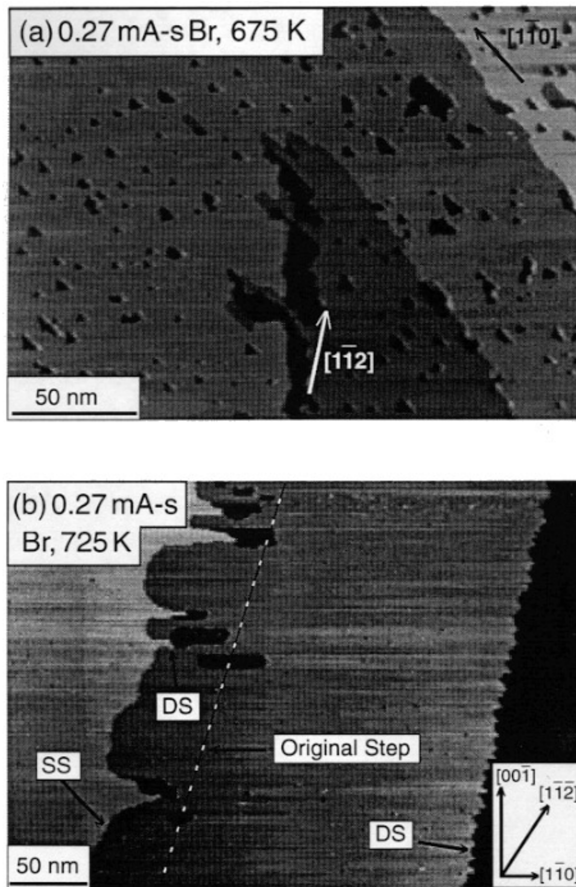

Figure 8. STM images revealing step etching. (a) Image of the surface after Br_2 exposure at 675 K showing a [1$\bar{1}$0] step in the upper right and another that intersects a [1$\bar{1}$2] step at the centre. The [1$\bar{1}$2] step has been modified substantially but the [1$\bar{1}$0] step shows little evidence of etching. (b) Image obtained after Br_2 exposure at 725 K. The white line approximates the original position of the SH step, showing retreat to the left by ∼500 Å. The right portion of the image shows a DH step with local sawtooth structure. Note that the [1$\bar{1}$0] direction in (b) is along the x-axis. (Adapted from [10].)

3.7. Bilayer etching

A distinctive bilayer etching channel opens up at high etching temperatures. Figure 9(a) shows a typical terrace after exposure at 725 K where the pits are two layers deep (4 Å) and have well defined triangular shapes. Several of the DH pits have coalesced. Their boundaries are defined by an As-terminated [1$\bar{1}$0] step and somewhat less regular [$\bar{1}$12] and [1$\bar{1}$2] steps. Dual-bias imaging reveals that the atomic arrangement at these DH steps resemble {111} microfacets [10]. Figure 9(b) highlights a DH triangular pit that extends across ∼10 rows. It is interesting to note that similar bilayer formation has been observed in GaAs growth on GaAs(110) in the same temperature regime (715–725 K) [30]. Those authors suggested that DH steps are stabilized due to a reconstruction at the

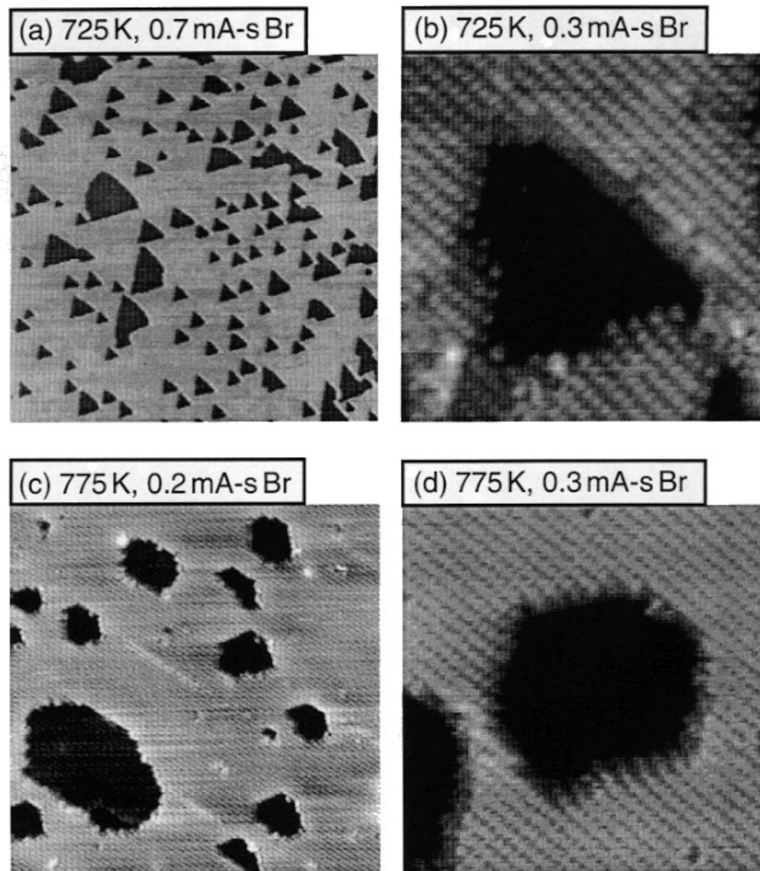

Figure 9. STM images representative of DH etching above 725 K. (a) Typical area on an extended terrace shows triangular double-layer pits. (b) Atomic resolution image of a DH pit bounded by $[\bar{1}12]$, $[1\bar{1}2]$ and $[1\bar{1}0]$ steps that form As{111} microfacets. (c) Etching by Br_2 exposure at 775 K leads to hexagonal DH pits plus extended SH pits. Both SH and DH structures are defined by As- as well as Ga-terminated steps. (d) An atomic resolution image of a typical DH etch pit with sixfold symmetry. It is bounded by Ga- and As{111} facets. ((a) 3000×3000 Å^2, (b) 110×110 Å^2, (c) 400×400 Å^2, (d) 140×140 Å^2.) (Adapted from [10].)

step edges. The etching studies show a reconstruction with $n\times$ ($n = 2$–4) periodicity at the As$[1\bar{1}0]$ steps [10, 12]. These observations suggest that reconstructions at DH steps do play an important role in determining the growth and etching profiles in the bilayer regime.

An increase in the etching temperature to 775 K results in DH pits that exhibit sixfold rather than threefold symmetry, as in figures 9(c) and 9(d). The high resolution image of figure 9(d) shows a DH pit when three of the sides are still {111} facets with DH $[1\bar{1}2]$, $[\bar{1}12]$ and As-terminated $[1\bar{1}0]$ steps. We suggest that the change implies that the etching anisotropy regarding Ga- and As-terminated {111} facets is curtailed at higher temperatures. By inference, the three original DH {111} facets are As terminated and the three facets exposed at higher temperature and flux are Ga-terminated. We note that Furuhata *et al* [31]

observed that the macro-etch rate for {111} Ga- and As-terminated planes are nearly equal for Cl_2 dry etching of GaAs above ~725 K, consistent with our observation of hexagonal etch pits. From the lower part of figure 9, it is apparent that single layer etching is still possible and the resultant pits increasingly show hexagonal shapes. This is consistent with the picture where Ga and As steps (DH or SH) exhibit similar etching behavior in this temperature regime.

Continuous etching in the DH regime favours lateral growth and coalescence of pits without much etching into the exposed terrace to form pits within pits [10]. In this regime, it is possible to obtain relatively smooth post-etch surfaces via bilayer-by-bilayer removal. Single-layer-by-single-layer removal can be achieved by an expose/anneal cycle followed by continued etching under well tuned conditions [32].

Figure 10 summarizes the results for thermally activated continuous etching of GaAs(110) by Br or Cl under conditions of low flux and submonolayer coverages. With increasing temperature, the surface concentration decreases under conditions of constant flux. The principal difference between Br and Cl is that there is an overall temperature reduction of 25–50 K to reach the same etching regime. In the lower temperature etching regime, GaX_3 is the dominant desorption product, together with As_2. At higher temperature, the GaBr channel dominates. In particular, several reaction pathways have been identified. These results show that it is possible to vary the surface morphologies by changing etching parameters of flux, fluence and temperature. Surface morphologies can also be engineered by following different scenarios, such as TPD versus continuous etching. In the following section, we discuss the effects of photon irradiation.

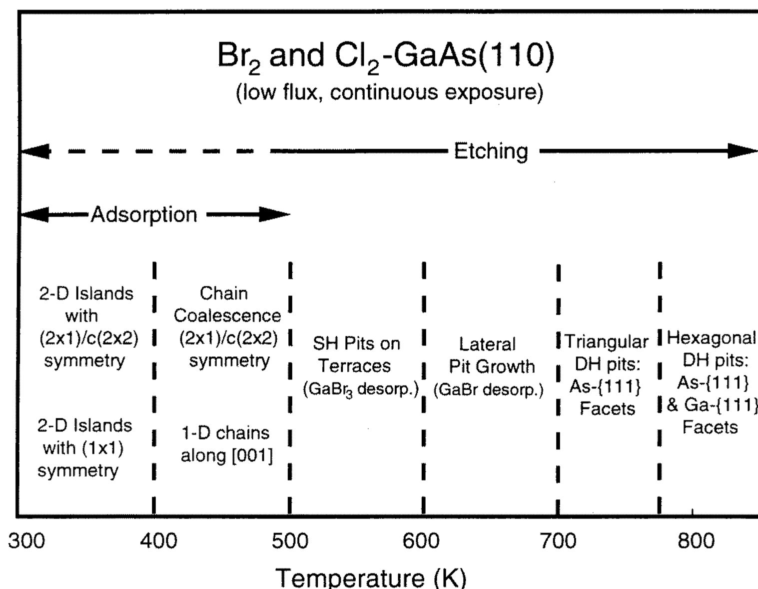

Figure 10. Schematic summary of halogen interaction with GaAs(110) under conditions of low flux at temperatures indicated. Under these conditions, the surface concentration decreases with increasing temperature. The boundaries between the different phases are not intended to be sharp. Transitions from one structure to the other are gradual and only the dominant behavior is given. The dashed line part of the domain implies much reduced etching.

4. Pulsed-laser-enhanced etching

The development of pulsed lasers opened up a new area of materials synthesis and processing. Pulsed lasers have been used in ablation for thin film synthesis, in precise film thickness trimming and in semiconductor etching [33]. Important work has focused on the processes involved in laser-activated surface chemistry and in etching [33, 34]. However, the experimental investigations have emphasized the reaction products and have provided limited information about the surface structure.

A recent STM study by Cha *et al* [13] revealed that pulsed-laser-induced etching of Br–GaAs(110) results in very different pit morphologies comparing to those obtained from spontaneous etching. The starting surfaces had a coverage of ~0.3 ML of Br chemisorbed at 450 K, resulting in structures with elongation along [001], as in figure 1(c). They were then irradiated with the light pulses from an Nd:YAG laser ($h\nu = 2.3$ eV) or heated to 700 K for 20 min. The results shown in figure 11(a) were obtained after irradiation with

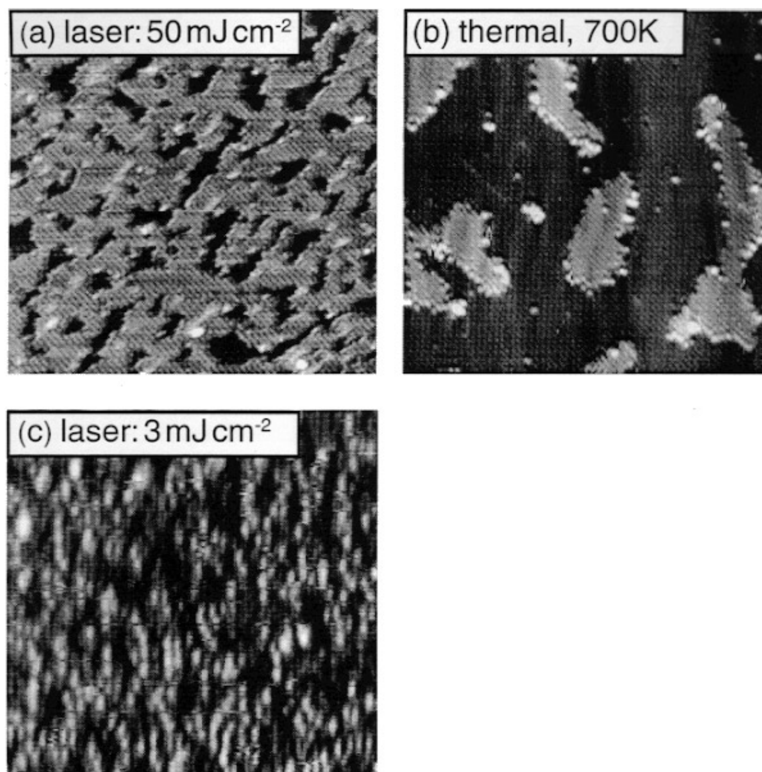

Figure 11. Surface morphologies obtained with laser and thermal activation. (a) Irradiation of a surface covered with ~0.3 ML Br by ~1.2×10^4 laser pulses ($h\nu = 2.3$ eV, pulse energy fluence ~50 mJ cm^{-2}, pulse duration ~6 ns) produces narrow etch pits that are elongated along [001] but are only a few Ga–As pairs in width. About 20% of the top layer has been removed. (b) Annealing of a surface with the same initial Br coverage to 675 K leads to a very different morphology where 60% of the top layer has been removed. (c) Irradiation of a surface that was nearly saturated with Br, as in figure 1(d), by ~7.2×10^4 laser pulses with a pulse energy fluence of ~3 mJ cm^{-2} produces scattered etch pits (dark areas). ((a) 540×540 Å^2, (b) 400×400 Å^2, (c) 250×250 Å^2.) (Adapted from [13].)

$\sim 1.2 \times 10^4$ pulses with a pulse intensity of $\sim$50 mJ cm^{-2}. It is evident that the terrace pits exhibit the same shape anisotropy as the chemisorption islands, with a comparable aspect ratio and elongation along [001]. Typical pits cross $\sim$10 zig-zag rows but are only a few Ga–As pairs in width. The amount of material removed was $\sim$0.2 ML. Since the starting surface was covered with 0.3 ML of Br and most of it was removed by irradiation, we conclude that about two surface atoms were removed for every three Br atoms. Control experiments showed that exposure of Br-free GaAs(110) to the same laser fluence resulted in no surface modification. The surface imaged in figure 11(b) was exposed to the same amount of Br at 450 K but it was then heated to 700 K. In this case, extensive portions of the first layer were removed and there were few isolated pits. Pit boundaries are made up of straight sections of steps parallel to $[1\bar{1}0]$ and highly kinked steps that cross $[1\bar{1}0]$. This thermal etching resulted in $\sim$0.6 ML removal, three times as high as with laser etching. The structures achieved by laser activation are highly irregular and represent a much higher surface energy configuration than those reached by thermal etching at 700 K.

For GaAs, the dominant absorption mechanism for 2.3 eV photons involves creation of electron–hole pairs [33, 35]. The photocarriers can initiate or enhance surface reactions by substrate-to-surface charge transfer processes [35], as demonstrated by Ashby [36] for GaAs in aqueous and gaseous environments. However, for intense pulsed laser irradiation, most of the excitation energy is expected to be transformed within nanoseconds into heat in the near-surface region due to increased electron–electron and electron–phonon scattering [33]. In a pump–probe experiment, Hicks *et al* [37] demonstrated that a classical heat diffusion model [38] can be used to describe pulsed surface heating for metals.

According to the one-dimensional heat diffusion model, the increase in surface temperature is given by $\Delta T = F[(1-R)/(cd)]$ and the duration is $\tau = d^2/4D_t$. Here, d is the initial excitation depth [39], c is the specific heat, F is the laser pulse power, R is the reflectivity and D_t is the thermal diffusivity. The parameters for GaAs and 2.3 eV irradiation are $d = 5 \times 10^{-5}$ cm, $c = 1.86$ J cm^{-3} K^{-1}, $R = 0.35$, and $D_t = 0.24$ cm^2 s^{-1} [40]. For a laser fluence of 50 mJ cm^{-2}, the temperature increase would be roughly $\Delta T = 300$–400 K. We know that etching via $GaBr_3$ desorption starts at $\sim$500 K and via GaBr desorption at $\sim$600 K for submonolayer coverage (see figure 4). Accordingly, a peak temperature of 600–700 K would be more than sufficient to induce etching.

The STM profiles indicate that Br surface diffusion is suppressed during laser etching. This becomes evident by considering the average diffusion distance $l(\tau)$ for a Br adatom during the pulse, as estimated from the classical surface diffusion model with $l(\tau) = (D\tau)^{1/2}$ and $D = 1/4[a^2\nu\exp(-E_d/kT)]$ where D is the diffusivity, a is the jump distance, E_d is the diffusion barrier and ν is the attempt frequency. Assuming that the surface temperature is 700 K for 10 ns, that $a = 4$ Å (the As–As distance along $[1\bar{1}0]$), that $E_d = 0.5$ eV [20] and that $\nu = 10^{13}$ s^{-1}, then the diffusion length is only $\sim$8 Å. This probably overestimates $l(\tau)$ since it is based on E_d for unhindered motion on a pristine surface along $[1\bar{1}0]$. For those Br adatoms inside chemisorption islands, diffusion would involve a very different potential energy surface than for the pristine surface.

So far we have discussed laser etching in the context of pulsed thermal activation. To assess the importance of electronic contributions, Cha *et al* [13] reduced the laser power to $\sim$3 mJ cm^{-2}. With this fluence, the surface temperature rise was only 20 K, too low to activate thermal etching. Figure 11(c) represents a surface with 0.6 ML Br after irradiation with 7.2×10^4 pulses. Note that this surface was exposed to Br_2 at 300 K to minimize the possibility of spontaneous etching, even though low temperature chemisorption produced less ordered 2×1/c(2×2) Br structures. Extensive irradiation produced dark patches

that decorate the surface. Accordingly, there are non-thermal electronic processes that are involved in the observed etching.

Electronic excitation mechanisms are activated where photogenerated electrons and holes reach the surface. Cierocki *et al* [17] have assigned valence band photoemission features of Br–GaAs(110) to bonding and antibonding combinations of halogen p orbitals with dangling sp^3 orbitals of the surface. The Br–Ga and Br–As bonding states are 3.2 eV and 4.7 eV below the valence band maximum (VBM), respectively, as sketched in figure 12. Those authors located the antibonding (Br–As)* state 0.28 eV above the VBM. Since this was the only adsorbate state found in the gap, they assumed that the antibonding (Br–Ga)* level fell within the conduction band. Within that framework, it is possible to envision excitation of Br–Ga and Br–As bond vibrations in terms of populating and depopulating Br adsorbate states. Such excitations are a prerequisite for desorption. Since the bonding orbitals are deep in the valence band, they are always occupied (the photon energy is too low to deplete them). Hence, it is the change in occupancy of (Br–As)* and (Br–Ga)* levels that could induce adsorbate vibrations.

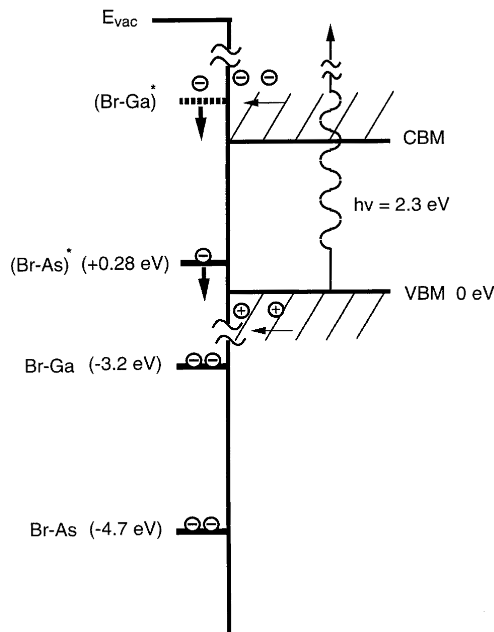

Figure 12. Band diagram for GaAs that illustrates transfer of photogenerated carriers to Br-induced adsorbate states under the flat-band conditions established by the surface photovoltage. The adsorbate energies are from [17]. (Adapted from [13].)

The band picture of figure 12 is drawn for a flat-band configuration. Under equilibrium conditions, there would be band bending to account for occupancy of the (Br–As)* states. Such band bending would influence the migration of electrons and holes. Accordingly, photocarrier-induced reactions would show a pronounced dependence of the etch yield on dopant type [35]. However, for nanosecond pulses with more than 1 mJ cm^{-2} per pulse, the photocarrier density in the depletion region exceeds the dopant concentration by orders of magnitude and flat-band conditions that result from a surface photovoltage would prevail. Hence, the generic bands in figure 12 can be drawn without specifying the Fermi level position. It also explains why Cha *et al* did not observe an etch yield difference between n- and p-doped samples.

Following laser irradiation, holes in the valence band can migrate to the surface and recombine with trapped charge in (Br–As)* states. Energetic conduction band electrons can

populate the (Br–Ga)* states. Electrons pumped into (Br–Ga)* states can recombine with holes, and the (Br–As)* states can be re-populated by photogenerated electrons. During irradiation, the surface electronic system is far from equilibrium as surface orbitals are subject to one or more population–depletion cycles via transfer and recombination. This leads to excitation of adsorbate vibrations that are necessary for initiating a backbond-breaking reaction. It should be noted, of course, that the simple band picture depicted in figure 12 is complicated by the fact that there are states associated with steps and kinks, and desorption of Ga or As via a monobromide channel is energetically favoured at a step compared to a terrace.

From figure 11(c), it is apparent that laser-enhanced etching with 3 mJ cm^{-2} at $\sim$300 K is not very efficient. Since laser-enhanced etching represents a combination of surface heating and electronic excitation of the adsorbate–substrate system, it is instructive to examine the desorption yield per pulse as a function of laser power and ambient temperature to quantify these contributions [41].

5. Concluding remarks

The morphologies for halogen-etched GaAs(110) reflect temperature-dependent etching pathways. Terrace etching sets in at $\sim$500 K with desorption of GaX_3 (X = Br, Cl) and formation of single layer etch pits. Significant lateral enlargement of etch pits sets in at $\sim$600 K with desorption of GaX. Terrace pit formation and growth primarily involves pairwise removal of Ga–As from zig-zag rows of the surface lattice. When terrace pits grow larger, they tend be bounded by segments of $[1\bar{1}0]$ steps and kinked $\langle 1\bar{1}2 \rangle$ boundaries. A distinct etching channel, characterized by double-layer removal fashion and triangular shapes, sets in at about 700 K for Br–GaAs(110). The corresponding onset for Cl–GaAs(110) is at about 650 K. The double height triangular pits are bounded by $\langle 1\bar{1}2 \rangle$ and $\langle 1\bar{1}0 \rangle$ steps and expose As-terminated {111} microfacets. A further increase of temperature leads to hexagonal pits bounded by both As- and Ga-terminated {111} facets. Nanosecond laser-pulse ($h\nu = 2.3$ eV) irradiation of Br-covered GaAs(110) results in very different etch pit morphologies comparing to those obtained in spontaneous etching. This laser-induced etching can be explained by a combination of short-duration substrate heating and substrate-mediated charge transfer processes. It occurs under conditions where surface diffusion of Br is minimal so that the pit profiles reflect the chemisorption structures.

We demonstrate that these surface morphology studies using high-resolution scanning tunnelling microscopy complement previous reaction product studies about halogen etching of III–V compound semiconductors. A combination of both allows us to obtain a comprehensive picture of some basic processes in the etching reactions.

Acknowledgments

This work was supported by the Army Research Office. We gratefully acknowledge the contributions from the Electronic Materials Group at the University of Minnesota, past and present.

References

[1] For recent reviews, see Winters H F and Coburn J W 1992 *Surf. Sci. Rep.* **14** 161
Yu M L and DeLouise L A 1994 *Surf. Sci. Rep.* **19** 285
[2] French C L, Balch W S and Foord J S 1991 *J. Phys.: Condens. Matter* **3** S351

[3] Tyrrell G C, Marshall D, Beckman J and Jackman R B 1991 *J. Phys.: Condens. Matter* **3** S179
[4] Su C, Hou H-Q, Lee G H, Dai Z-G, Luo W, Vernon M F and Bent B E 1993 *J. Vac. Sci. Technol.* B **11** 1222
[5] Balooch M, Olander D R and Siekhaus W J 1986 *J. Vac. Sci. Technol.* B **4** 794
[6] McLean A B, Terminello L J and McFeely F R 1989 *Phys. Rev.* B **40** 11 778
[7] Gu C, Chen Y, Ohno T R and Weaver J H 1992 *Phys. Rev.* B **46** 10 197
[8] Stepniak F, Rioux D and Weaver J H 1994 *Phys. Rev.* B **50** 1929
[9] Shuh D K, Lo C W, Yarmoff J A, Santoni A, Terminello L J and McFeely F R 1994 *Surf. Sci.* **303** 89
[10] Patrin J C and Weaver J H 1993 *Phys. Rev.* B **48** 17 913
Patrin J C, Li Y Z, Chander M and Weaver J H 1993 *Appl. Phys. Lett.* **62** 1277
[11] Cha C Y, Brake J, Han B Y, Owens D W and Weaver J H 1997 *J. Vac. Sci. Technol.* B **15** 605
Brake J, Cha C Y, Han B Y, Owens D W and Weaver J H 1997 *J. Vac. Sci. Technol.* B **15** 670
[12] Han B Y, Cha C Y and Weaver J H 1997 *Phys. Rev.* B **56** 4966
[13] Cha C Y, Han B Y and Weaver J H 1997 *Surf. Sci.* **381** L636
Han B Y, Cha C Y and Weaver J H 1998 *J. Vac. Sci. Technol.* A **16** 490
[14] Spencer N D, Goddard P J, Davies P W, Kitson M and Lambert R M 1983 *J. Vac. Sci. Technol.* A **1** 1554
[15] See Flaum H C, Sullivan D J D and Kummel A C 1994 *J. Chem. Phys.* **100** 1634. Using molecular beam techniques, they derived an initial sticking probability of 0.52–0.74 for Cl_2 (translational energy 0.02–0.6 eV) impinging at normal incidence on GaAs(110) at 300 K.
[16] Margaritondo G, Rowe J E, Bertoni C M, Calandra C and Manghi F 1979 *Phys. Rev.* B **20** 1538
Margaritondo G, Rowe J E, Bertoni C M, Calandra C and Manghi F 1981 *Phys. Rev.* B **23** 509
[17] Cierocki K, Troost D, Koenders L and Mönch W 1992 *Surf. Sci.* **264** 23
[18] Corkill J L and Chelikowsky J R 1994 *Phys. Rev.* B **50** 11 924
Corkill J L and Chelikowsky J R 1996 *Phys. Rev.* B **53** 12 605
[19] Khoo G S and Ong C K 1994 *Phys. Rev.* B **50** 10 796
[20] In [18] Corkill and Chelikowsky estimated the diffusion barrier for Cl atoms on GaAs(110) terraces to be ~0.5 eV along $[1\bar{1}0]$ and ~1.5 eV along [001].
[21] Feenstra R M, Stroscio J A, Tersoff J and Fein A P 1987 *Phys. Rev. Lett.* **58** 1192
[22] McCoy J M and LaFemina J P 1996 *Phys. Rev.* B **54** 14 511
[23] Biegelson D K, Bringans R D, Northrup J E and Swartz L-E 1990 *Phys. Rev. Lett.* **65** 452
[24] Haberern K W and Pashley M D 1990 *Phys. Rev.* B **41** 3226
[25] Hashizume T, Xue Q K, Zhou J, Ichimiya A and Sakurai T 1994 *Phys. Rev. Lett.* **73** 2208
Hashizume T, Xue Q K, Ichimiya A and Sakurai T 1995 *Phys. Rev.* B **51** 4200
[26] Behrend J, Wassermeier M, Däweritz L and Ploog K H 1995 *Surf. Sci.* **342** 63
[27] Kim H and Chelikowsky J R 1996 *Phys. Rev. Lett.* **77** 1063
[28] Zhang S B and Zunger A 1996 *Phys. Rev. Lett.* **77** 119
[29] Ihm J and Joannopoulos J D 1982 *Phys. Rev.* B **26** 4429
[30] Fawcett P N, Neave J H, Zhang J and Joyce B A 1993 *Surf. Sci.* **296** 67
[31] Furuhata N, Miyamoto H, Okamoto A and Ohata K 1990 *J. Electron. Mater.* **19** 201
[32] Cha C Y and Weaver J H 1996 *J. Vac. Sci. Technol.* B **14** 3559
[33] See Ashby C I H and Tsao J Y 1989 *Laser Microfabrication* ed D J Ehrlich and J Y Tsao (San Diego, CA: Academic) and references therein
[34] Chuang T J 1983 *Surf. Sci. Rep.* **3** 1
[35] Morrison S R 1990 *Chemical Physics of Surfaces* (New York: Plenum)
[36] Ashby C I H 1984 *Appl. Phys. Lett.* **45** 892
Ashby C I H 1985 *Appl. Phys. Lett.* **46** 752
[37] Hicks J M, Urbach L E, Plummer E W and Dai H-L 1988 *Phys. Rev. Lett.* **61** 2588
[38] Baeri P, Campisano S U, Foti G and Rimini E 1979 *J. Appl. Phys.* **50** 788
[39] The initial excitation depth is the thickness of the surface layer in which the photon energy is converted into lattice heat. From [33], it is the longer of the optical absorption length (about four times the reciprocal of the optical absorption coefficient) or the thermal diffusion length, $[2D_t\tau]^{1/2}$ where D_t is the thermal diffusivity and τ is the thermal pulse length. Both distances are about 5×10^{-5} cm for GaAs with 6 ns, 2.3 eV laser pulses.
[40] Sze S M 1981 *Physics of Semiconductor Devices* (New York: Wiley)
[41] Han B Y and Weaver J H 1998 *Phys. Rev.* B at press